Characterisation of composite elastic properties by means of a multi-scale two-level inverse approach

Lorenzo Cappelli[a], Marco Montemurro[a,*], Frédéric Dau[a], Laurent Guillaumat[b]

[a] Arts et Métiers ParisTech, Institut de Mécanique et d'Ingénierie (I2M) de Bordeaux CNRS UMR 5295, F-33400 Talence, France
[b] Arts et Métiers ParisTech, Laboratoire angevin de mécanique, procédés et innovation (LAMPA), F-49100 Angers, France

Keywords:
Composite material
Homogenisation
Optimisation
Harmonic analysis
Inverse problems
Identification

A B S T R A C T

This work deals with the problem of characterising the elastic properties of a composite material at both mesoscopic (ply-level) and microscopic (constitutive phases-level) scales. This goal is attained by means of an adequate multi-scale identification strategy (MSIS) which aims at identifying the constitutive properties, at each relevant scale, by exploiting the information restrained in the macroscopic dynamic response of the composite. In this background, the multi-scale identification problem is split into two interdependent sub-problems which are stated, at both levels, as constrained minimisation problems. At the first level the goal is the characterisation of the lamina properties by minimising the distance between the numerical and the reference harmonic responses of the composite. The second level problem aims at identifying the elastic properties of both fibre and matrix by minimising the distance between the effective elastic properties evaluated through a homogenisation process and those provided by the first-level inverse problem. The MSIS is based on a special global hybrid optimisation tool and on the strain energy homogenisation method of periodic media. Its effectiveness is proven through a meaningful benchmark.

1. Introduction

Nowadays, composite materials are widely used in several fields, from automotive applications to aerospace ones. This is mainly due to their high stiffness/mass and strength/mass ratios when compared to steel or aluminium alloys. Furthermore, engineers are continuously looking for strategies that allow increasing performances, building integrated and lighter structures, designing complex geometry and providing stiffness and strength where needed.

Nevertheless, in order to properly conceive complex and optimised solutions, it is mandatory to characterise the full set of the composite material properties at each pertinent scale. One of the main issues of composite materials is related to the difficulty of characterising the full set of elastic properties at the lower scales, i.e. microscopic (that of the constitutive phases) and mesoscopic (the lamina level) ones.

Indeed, it is very interesting, especially from an industrial point of view, to be able to reduce the cost of experimental characterisation tests which are usually destructive procedures. Such tests must be carried out on a significant number of samples in order to get reliable results (thus leading to quite expensive experimental campaigns) [1]. Moreover, as far as concerns the characterisation of the elastic properties of the constitutive phases, a large data dispersion is obtained during micro-scale experimental tests, due to the difficulty to properly set the experiment and to handle the microscopic constituents [2].

Concerning the experimental (destructive) tests, they can be divided into meso and micro-scale characterisation tests. The most important meso-scale tests are: (1) the tension test for flat specimens (ASTM D3039 [3]); (2) three/four points bending test (ASTM D790 [4]); (3) compression tests (shear loading methods ASTM D3410 [5]; (4) end loading methods ASTM D695 [6]; (5) combined loading methods ASTM D6641 [7]); (6) shear tests (in-plane shear tests ASTM D5379 [8]-D7078 [9]-D3518 [10], out-of-plane - interlaminar shear tests ASTM D2344 [11]-D5379).

Nevertheless, ASTM standard tests conducted at the lamina level are not able to provide the full set of 3D elastic properties: only the in-plane material properties together with an approximated value of the out-of-plane shear moduli can be retrieved through these tests.

Conversely, only few standard tests can be carried out at the microscopic scale: single fibre test to obtain the Young's modulus along the fibre longitudinal direction (ASTM D3379 [12]) and matrix tensile test (ASTM D638 [13]). In order to characterise the rest of the constitutive phases properties, only non-standard tests are available in literature: pull-out [14], micro-indentation [2], fragmentation tests [15], etc.

* Corresponding author.
E-mail addresses: marco.montemurro@ensam.eu, marco.montemurro@u-bordeaux.fr (M. Montemurro).

https://doi.org/10.1016/j.compstruct.2018.08.007

When looking at the determination of the elastic properties of the microscopic phases, the limitations related to ASTM tests and/or unconventional destructive tests become more important. On the one hand, ASTM tests can provide information (with a high level of dispersion) only about the Young's modulus along fibre axis and matrix in-plane properties. The rest of the elastic properties (especially those of the fibre) cannot be retrieved by means of ASTM tests. On the other hand, also unconventional destructive tests, often used to characterise the matrix-fibre interface properties, present some major shortcomings: the experimental set-up is quite complex and, even when the experiment is properly realised, the obtained results show a significant dispersion (results are very sensitive to boundary conditions and edge effects related to the experimental set-up), see [16].

In order to go beyond the main restrictions imposed by destructive tests, the research activity here presented focuses on the development of a multi-scale identification strategy (MSIS), based on non-destructive tests, able to characterise the elastic properties of the composite at each relevant scale, namely microscopic and mesoscopic ones.

The main idea behind this approach is quite simple: the proposed MSIS aims at identifying the full set of elastic properties at both lamina-level and constitutive phases-level starting from the analysis of the *macroscopic* dynamic response of a multilayer plate. In particular, the macroscopic dynamic behaviour can be easily obtained by means of non-destructive modal tests: the information restrained in the harmonic spectrum response of the specimen can be then exploited to carry out the multi-scale characterisation process.

It is noteworthy that the utilisation of identification strategies exploiting the information restrained in a macroscopic modal analysis is not new. This kind of approach has already been applied in literature [17–21] for characterising the elastic properties of the constitutive lamina. An assessment of these approaches is available in [22,23]. Most of these techniques, e.g. that proposed in [24], make use of an optimisation tool (generally a gradient-based algorithm) in order to minimise the difference between the measured dynamic response (typically a given set of natural frequencies) and the numerical one calculated via a finite element (FE) model of the structure.

However, to the best of the authors' knowledge, this approach has never been generalised to characterise the material and geometrical features of the microstructure of composite materials.

Indeed, in the context of the proposed approach, the material characterisation problem is split into two distinct (but related) sub-problems. The first level of the procedure focuses on the transition from macroscopic scale to mesoscopic one and aims at minimising the distance between the *reference* harmonic response of the structure and its numerical counterpart: the goal is to search for the elastic properties of the constitutive ply minimising this distance. The second step focuses on the transition from mesoscopic scale to microscopic one: the goal is the determination of both geometrical and elastic properties of the constitutive phases meeting the lamina elastic properties resulting from the first-level inverse problem.

The MSIS is characterised by several original features. On the one hand, it relies on a special hybrid optimisation tool to perform the solution search, i.e. an in–house code made by the union of a special genetic algorithm (GA) (able to deal with problems characterised by a *variable number of design variables* [25]) and of a classical gradient-based one. On the other hand, the link between the two identification problems (stated at different scales) is ensured by a general numerical homogenisation scheme: the one utilising volume-averaged stresses determined on a suitable representative volume element (RVE) of the material in the framework of the strain energy method of periodic media [26].

The paper is structured as follows: the problem and the MSIS are introduced in Section 2. The mathematical formulation of the inverse problem at the ply-level and the related numerical aspects are discussed in Section 3, while the micro-scale characterisation problem as well as the numerical homogenisation scheme (and the related FE model) are discussed in Section 4. The numerical results of the MSIS are illustrated and discussed in Section 5. Finally, Section 6 ends the paper with some conclusions and perspectives.

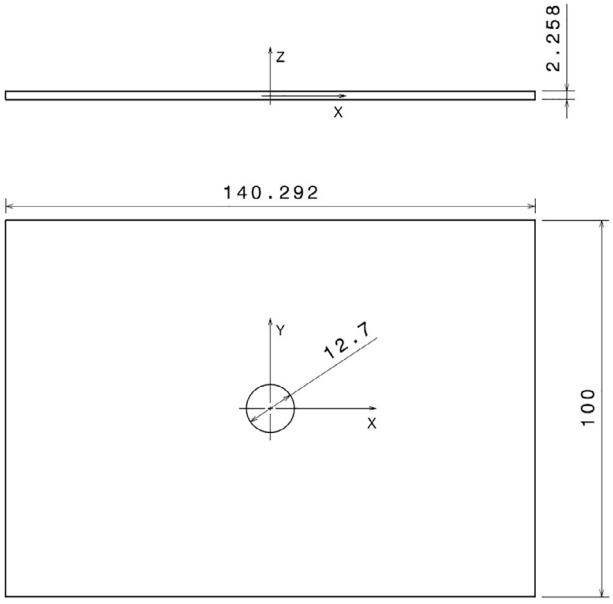

Fig. 1. Geometry of the multilayer composite plate (sizes in [mm]).

2. Multi-scale identification of composite elastic properties

2.1. Problem description

The multi-scale inverse approach presented in this study is applied to a reference multilayer composite plate made of unidirectional laminae whose geometry is illustrated in Fig. 1.

The constitutive ply is made of carbon-epoxy fibre Hexcel $T650/F584$ pre-impregnated tapes, with a fibre volume fraction $V_f = 0.555$: the material properties of the constitutive phases composing the ply (taken from [27]) are listed in Table 1. As it can be noticed, the fibre has a transverse isotropic behaviour, while the matrix is isotropic.

The reference laminate is constituted of eight identical plies (i.e. same material and thickness) arranged according to the following stack $[0°/-45°/45°/90°]_S$. The thickness of the lamina is $t_{ply} = 0.28225$ mm. The orientation angle of the generic ply is positive according to counter-clockwise rotation around the z-axis: x-axis indicates the 0° orientation.

The analysis presented in this work constitutes a numerical validation of the MSIS: the *reference response* of the structure (at each scale) is determined by means of a multi-scale numerical analysis on the reference configuration of the laminate described above.

In particular, as described in Section 5.1, the reference material properties of the constitutive phases are used in order to calculate, on the one hand, the *reference effective elastic properties* of the lamina at the mesoscopic scale and, on the other hand, the *reference harmonic response* and the *reference natural frequencies* of the multilayer plate (macroscopic scale).

Concerning the microscopic scale the following hypotheses apply:

Table 1
Micro-scale reference material properties for the fibre $T650/35{-}3K$ and the matrix $F584$ (taken from [27,28]).

Fibre properties		Matrix properties				
E_1^f [MPa]	E_2^f [MPa]	ν_{12}^f	ν_{23}^f	G_{12}^f [MPa]	E_m [MPa]	ν_m
276000.0	17300.0	0.250	0.428	11240.0	4140.0	0.350

- the material of both constitutive phases has a linear elastic behaviour;
- perfect bonding condition at the fibre-matrix interface is considered;
- the damping capability of both phases is disregarded.

As far as mesoscopic and macroscopic scales are concerned, the following assumptions are made:

- the constitutive lamina has an elastic orthotropic behaviour;
- perfect bonding condition at the interface between two consecutive plies;
- the damping properties of the ply are neglected;
- the laminate kinematic is described in the framework of the first-order shear deformation theory (FSDT).

2.2. The multi-scale identification strategy

The main goal of the MSIS is to find the material properties of the considered structure at each relevant scale by exploiting the information restrained in the macroscopic dynamical response of the composite. The reference response can be provided either by a non-destructive harmonic test or by a numerical harmonic analysis conducted on a reference structure. This latter is the case considered in the present study: the reference configuration of the multilayer plate as well as the reference dynamical results are presented in Section 5.

In this background, the problem of characterising the elastic properties of the composite at different scales can be split into two distinct (but related) *inverse problems*.

- **First-level inverse problem**. This phase involves the transition from macroscopic scale (laminate-level) to mesoscopic one (ply-level): the goal is to characterise the ply elastic properties (the design variables of this phase) minimising the distance between the numerical harmonic response of the multilayer plate and the reference one.
- **Second-level inverse problem**. This step focuses on the transition from mesoscopic scale to microscopic one (that of the constitutive phases): the goal is to find the optimum value of elastic properties of both fibre and matrix (the optimisation variables of this phase) meeting the set of the lamina elastic properties provided by the first-level problem. In this second phase, the link between the two scales is ensured by means of a homogenisation analysis performed on the numerical model of the RVE of the material in order to compute the effective elastic properties of the ply.

The general architecture of the two-level MSIS is shown in Fig. 2.

3. Mathematical formulation of the first-level inverse problem

3.1. Optimisation variables, objective function and constraints

As stated above, the first-level inverse problem concerns the macroscopic/mesoscopic scale transition. The aim of this phase is to characterise the elastic properties of the constitutive lamina. In this background, the identification problem is formalised as a classical inverse problem. The goal is to find the set of elastic properties of the ply (in the most general 3D case) minimising the distance between the reference dynamic response of the structure and that provided by the numerical model of the structure.

According to the general hypotheses recalled in Section 2, the constitutive ply has a linear elastic orthotropic behaviour. However, taking into account the fibres arrangement, only six parameters must be identified during this step. As illustrated in Fig. 6, the considered RVE is characterised by five planes of orthogonal symmetry implying the following relationships: $E_2 = E_3$, $G_{12} = G_{13}$ and $\nu_{12} = \nu_{13}$.

Therefore, all the meso-scale material parameters can be collected into the vector of design variables $\mathbf{x}^{\mathrm{I}}$ as follows:

$$\mathbf{x}^{\mathrm{I}} = \{E_1,\, E_2,\, G_{12},\, G_{23},\, \nu_{12},\, \nu_{23}\}. \tag{1}$$

It is noteworthy that the ply elastic properties cannot get arbitrary values, rather they have to satisfy a set of existence constraints in order to ensure the positive definiteness of the lamina stiffness tensor:

$$\begin{aligned} g_1^{\mathrm{I}}(\mathbf{x}^{\mathrm{I}}) &= \left|\nu_{12}\right| - \sqrt{\tfrac{E_1}{E_2}} < 0, \\ g_2^{\mathrm{I}}(\mathbf{x}^{\mathrm{I}}) &= \left|\nu_{23}\right| - \sqrt{\tfrac{E_2}{E_3}} < 0, \\ g_3^{\mathrm{I}}(\mathbf{x}^{\mathrm{I}}) &= 2{\cdot}\nu_{12}{\cdot}\nu_{13}{\cdot}\nu_{23}{\cdot}\tfrac{E_3}{E_1} + \nu_{12}^2{\cdot}\tfrac{E_2}{E_1} + \nu_{23}^2{\cdot}\tfrac{E_3}{E_2} + \nu_{13}^2{\cdot}\tfrac{E_3}{E_1} - 1 < 0. \end{aligned} \tag{2}$$

Moreover, the lamina elastic constants vary within the design space defined in Table 2, i.e. by introducing appropriate lower and upper bounds for each design variable. The lower and upper bounds are chosen equal to the 80% and the 120% of the reference material properties at meso-scale respectively (given in Table 4). Only the lower and upper bounds of the optimisation variable ν_{23} are set equal to the 85% and the 115% of the corresponding reference value, respectively.

Concerning the expression of the first-level objective function, an error estimator of the least-squares type has been chosen:

$$\Phi^{\mathrm{I}}(\mathbf{x}^{\mathrm{I}}) = \frac{1}{N_p{\cdot}N_s} \sum_{q=1}^{N_p} \sum_{r=1}^{N_s} \left[\left(\frac{f_r - f_r^{\mathrm{ref}}}{f_r^{\mathrm{ref}}} \right)^2 + \left(\frac{H_{r,q}(\mathbf{x}^{\mathrm{I}}) - H_{r,q}^{\mathrm{ref}}}{H_{r,q}^{\mathrm{ref}}} \right)^2 \right]. \tag{3}$$

In the previous equation, f_r is the r-th sampled frequency, while $H_{r,q}$ is the fast Fourier transform (FFT) of the frequency response function (FRF) determined at the q-th sample point of the multilayer plate and evaluated at the r-th sampled frequency. Of course, f_r^{ref}, $H_{r,q}^{\mathrm{ref}}$ are the same quantities evaluated on the reference configuration of the laminate.

N_s and N_p are the number of sampled frequencies and of sample points over the laminate plate (where the FRF is computed/measured), respectively.

In order to get a numerical harmonic spectrum really close to the reference one (and also to match the reference natural frequencies), a set of constraints on the laminate eigenfrequencies is considered:

$$g_{3+j}^{\mathrm{I}}(\mathbf{x}^{\mathrm{I}}) = \left| \frac{f_{jn} - f_{jn}^{\mathrm{ref}}}{f_{jn}^{\mathrm{ref}}} \right| - \epsilon_j \leqslant 0, \quad j = 1,\ \ldots, n_f. \tag{4}$$

In Eq. (4), n_f is the overall number of natural frequencies involved in the analysis (i.e. in the frequency range used for the determination of the FRF), whilst f_{jn} and f_{jn}^{ref} are the numerical and reference j-th eigenfrequency, respectively. ϵ_j is a user-defined tolerance on the relative error for each natural frequency: in this study a maximum relative error equal to 0.005 has been considered.

Finally, the first-level inverse problem can be stated as a classical constrained non-linear programming problem (CNLPP):

$$\begin{aligned} &\min_{\mathbf{x}^{\mathrm{I}}} \Phi^{\mathrm{I}}(\mathbf{x}^{\mathrm{I}}), \\ &\text{subject to:} \\ &g_j^{\mathrm{I}}(\mathbf{x}^{\mathrm{I}}) \leqslant 0, \quad j = 1, \ldots, n_f + 3. \end{aligned} \tag{5}$$

3.2. The macroscopic finite element model

A picture of the FE model of the multilayer plate at the macroscopic scale together with the applied loads and boundary conditions (BCs) is illustrated in Fig. 3. Such a FE model (developed within ANSYS® environment [29]) is built by using ANSYS® SHELL281 layered shell elements with eight nodes and six degrees of freedom (DOFs) per node. The kinematic model is that of the first-order shear deformation theory (FSDT) [30].

The choice of shell elements is due to the aspect ratio (between the

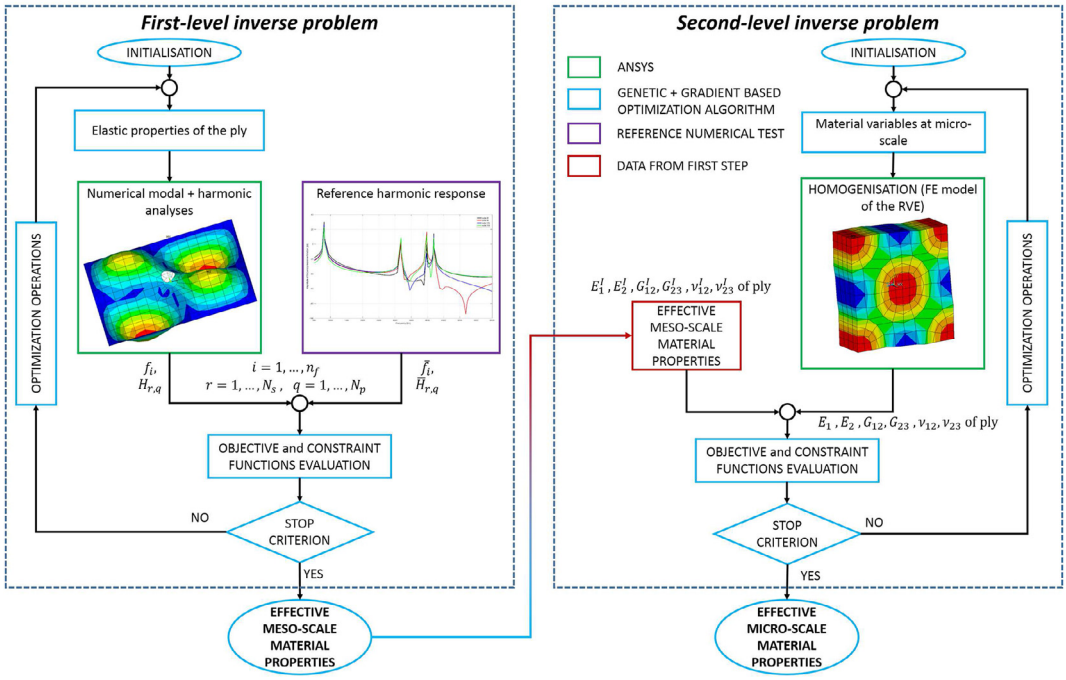

Fig. 2. The overall architecture of the MSIS.

Table 2
First-level inverse problem: design variables lower and upper bounds.

Ply elastic properties	Lower bound	Upper bound
E_1 [MPa]	124022.7	186034.1
E_2 [MPa]	6558.3	9837.4
ν_{12}	0.232	0.348
ν_{23}	0.433	0.586
G_{12} [MPa]	3069.7	4604.5
G_{23} [MPa]	2626.2	3939.3

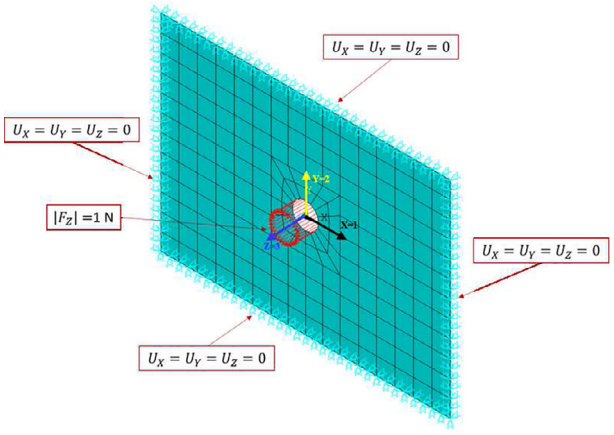

Fig. 3. FE model of the multilayer plate and the related BCs.

shortest edge length and the overall thickness) of the multilayer plate whose value, $AR = 44.29$, is in the range [20, 100] whereby the FSDT is well-suited to describe the laminate mechanical response.

During the optimisation process of the first step of the MSIS, two FE analyses are invoked for each point in the design space: firstly a modal analysis (eigenvalue analysis) to extract the first n_f natural frequencies and, secondly, a linear harmonic analysis in order to determine the harmonic response of the laminate. This latter is obtained by measuring the displacement u_z in each one of the q sample nodes of the mesh, at

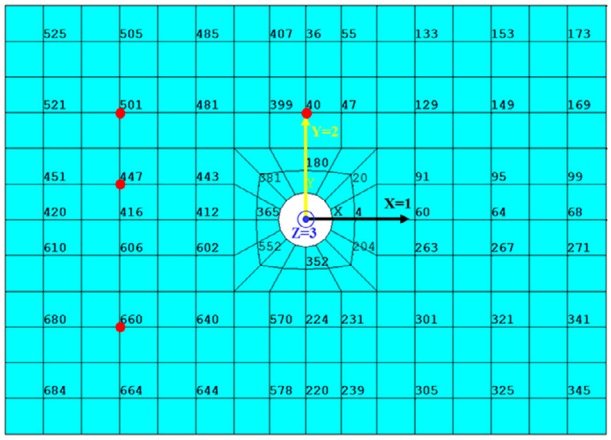

Fig. 4. Location of the sample points over the laminate used for harmonic displacements evaluation (the FRF related to nodes highlighted in red is shown in Fig. 9).

every sampled frequency f_r, as depicted in Fig. 4.

Subsequently, the FRF for each sample point is obtained by evaluating the ratio between the FFT of the displacement $u_{zq}(f_r)$ and that of the applied force $F_z(f_r)$, namely

$$H_{r,q} = \frac{u_{zq}(f_r)}{F_z(f_r)}. \tag{6}$$

It is noteworthy that, before starting the optimisation process two sensitivity studies (not reported here for the sake of brevity) have been conducted. The first one focused on the sensitivity of the system response with respect to the mesh size: it was observed that a mesh having 4176 DOFs, is sufficient to properly evaluate both the eigenfrequencies and the FRF of the laminate in each sample point. Conversely, the second sensitivity analysis aimed at investigating the influence of the number of sample points N_p on the overall FRF of the multilayer plate. It has been observed that an overall number of $N_p = 62$ sample points is sufficient to properly evaluate the global FRF of the structure.

Finally, as far as the linear harmonic analysis is concerned, the FFT of the structure in each sample point has been evaluated in the frequency range [500, 6000] Hz wherein $N_s = 82$ sampled spectrum frequencies have been considered, according to the strategy detailed in Section 5.

3.3. The numerical strategy

Problem (5) is highly non linear and non-convex in terms of both objective and constraint functions. Its non-linearity is mainly related to the expression of both objective and constraint functions, see Eqs. (2)–(4).

For inverse problems, the uniqueness of solution is not *a priori* guaranteed: the set of parameters matching a given *observed state* may not be unique. Nevertheless, no proved theoretical rules exist in literature [31,32] to define the number of data points N_p for a given number of unknowns (n) that have to be identified. Generally, the inverse problem is stated as a CNLPP and it can be viewed as an *over-determined system of equations* [31,32]. Since more observation points than parameters exist (N_p is usually much greater than n) there are more equations than unknowns. If an optimal point exists, of course it may be not unique, thus implying the existence of many combinations of parameters that result to be equivalent optimal solutions for the CNLPP at hand.

Considering all these aspects and according to the practice always employed in literature, in this work a number of observed states (i.e. sample points N_p) greater than two times the number of design variables n has been considered. As previously stated, the number of sample points has been inferred by means of a numerical sensitivity analysis of the FRF of the plate with respect to parameter N_p: as a results $N_p = 62$ has been chosen to properly perform the optimisation calculations.

Taking into account the previous aspects, a hybrid optimization tool composed of the new version of the GA BIANCA [33], interfaced with the MATLAB *fmincon* algorithm [34], has been used.

The GA BIANCA has already been successfully applied to solve different kinds of real-world engineering problems, see for instance [33,35–37].

As shown in Fig. 5, the optimisation procedure for problem (5) is split in two phases. During the first phase, solely the GA BIANCA is used to perform the solution search. Due to the strong non-linearity of problem (5), the aim of the genetic calculation is to provide a potential sub-optimal point in the design space, which constitutes the initial guess for the subsequent phase, i.e. the local optimisation, where the MATLAB *fmincon* tool is employed to finalise the solution search. The optimisation algorithm is the *active-set* which is a Quasi-Newton method making use of an approximation of the Hessian matrix to estimate the descent direction. For more details on the active-set algorithm see [34].

For the resolution of the first-level inverse problem, both optimisation algorithms have been interfaced with the FE model of the multilayer plate. As shown in Fig. 5, for each individual at each generation, the optimisation tool performs two FE analyses: a modal analysis to extract the n_f natural frequencies followed by a linear harmonic analysis for the evaluation of the FRF of the laminate. Then, the GA elaborates the results provided by the two FE analyses in order to execute the genetic operations on the basis of the current value of both objective and constraint functions. These operations are repeated until the GA BIANCA meets the user-defined convergence criterion.

The number of design variables and that of constraint functions is six and $n_f + 3$, respectively. The generic individual of the GA BIANCA represents a potential solution for the problem at hand. The genotype of the individual for problem (5) is characterised by only one chromosome composed of six genes, each one coding a component of the vector of design variables, see Eq. (1).

4. Mathematical formulation of the second-level inverse problem

4.1. Optimisation variables, objective function and constraints

As stated previously, the second-level inverse problem is focused on the transition from mesoscopic scale to microscopic one. The main purpose of this step is the characterisation of the elastic properties of the constitutive phases (i.e. fibre and matrix) by minimising the distance between the effective elastic properties of the constitutive lamina (determined numerically) and the reference ones (i.e. the optimum values) resulting from the first-level inverse problem, which represent the *reference response* for this phase.

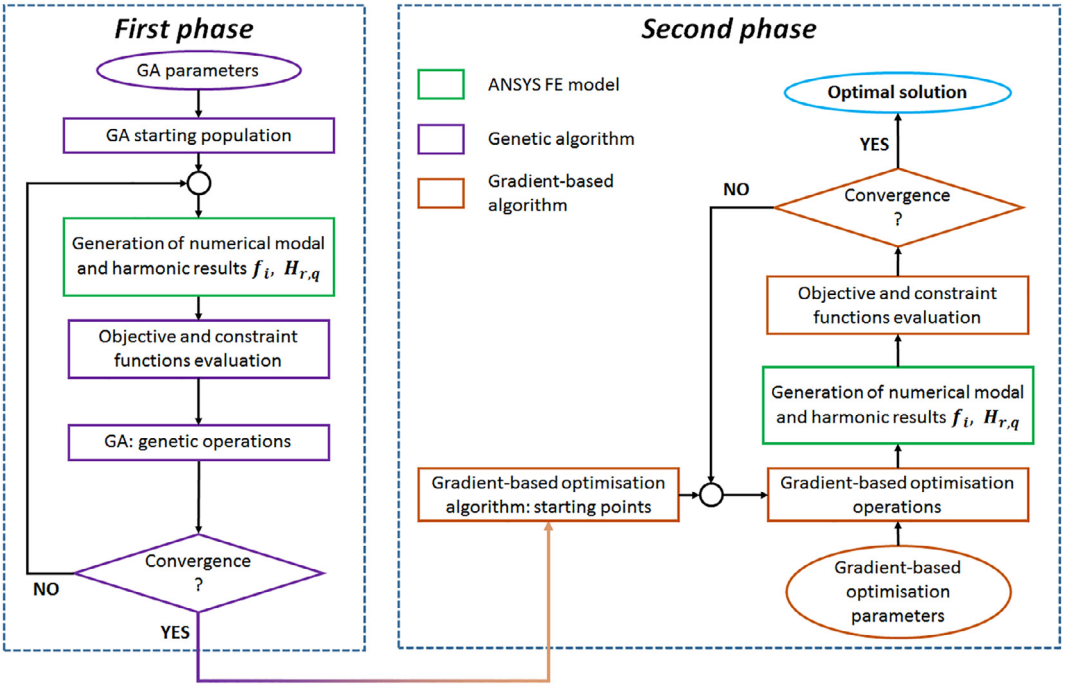

Fig. 5. Two-phases optimisation scheme for the first-level inverse problem.

Of course, the effective elastic properties of the lamina must be evaluated by means of a suitable homogenisation procedure. To this purpose, a FE model of the RVE of the composite is built in order to carry out the numerical homogenisation calculations which allow determining the equivalent meso-scale ply properties as a function of those of the constitutive phases. It is noteworthy that both geometrical and material parameters of the constitutive phases affect the equivalent material properties of the constitutive layer. Nevertheless, in the following the fibre volume fraction is set *a priori*, thus it is not considered among the design variables because it is always a reliable datum (always provided by the supplier in the specification sheet).

Considering the general hypotheses described in Section 2.1, the fibre has a linear elastic transverse isotropic behaviour while, the matrix has a linear elastic isotropic behaviour: only seven material parameters need to be identified. Therefore, these quantities are collected into the vector $\mathbf{x}^{\mathrm{II}}$ as follows:

$$\mathbf{x}^{\mathrm{II}} = \{E_1^f,\, E_2^f,\, G_{12}^f,\, \nu_{12}^f,\, \nu_{23}^f,\, E_m,\, \nu_m\}. \tag{7}$$

Similarly to the first-level inverse problem, the constitutive elastic properties cannot assume arbitrary values, but they have to fulfil a set of existence constraints to guarantee the positive definiteness of the fibre and matrix stiffness tensors:

$$\begin{aligned}
g_1^{II}(\mathbf{x}^{II}) &= \left|\nu_{12}^f\right| - \sqrt{\frac{E_1^f}{E_2^f}} < 0,\\
g_2^{II}(\mathbf{x}^{II}) &= |\nu_{23}^f| - 1 < 0,\\
g_3^{II}(\mathbf{x}^{II}) &= \frac{E_1^f}{E_2^f}\cdot(2\cdot\nu_{23}^f\cdot\nu_{12}^{f\,2} + 2\cdot\nu_{12}^{f\,2}) - 1 < 0,\\
g_4^{II}(\mathbf{x}^{II}) &= \nu_m - \frac{1}{2} < 0,\\
g_5^{II}(\mathbf{x}^{II}) &= -\nu_m - 1 < 0.
\end{aligned} \tag{8}$$

Furthermore, the components of the design variables vector can take values within the design space defined in Table 3, in which appropriate lower and upper bounds for each design variable are assigned. The lower and upper bounds are chosen equal to the 80% and the 120% of the reference material properties at micro-scale (given in Table 1), respectively.

Moreover, regarding the objective function expression, an error estimator of the least-square type has been chosen:

$$\begin{aligned}
\Phi^{II}(\mathbf{x}^{II}) = \frac{1}{6}\Bigg[&\left(\frac{E_1 - E_1^{\mathrm{I}}}{E_1^{\mathrm{I}}}\right)^2 + \left(\frac{E_2 - E_2^{\mathrm{I}}}{E_2^{\mathrm{I}}}\right)^2 + \left(\frac{G_{12} - G_{12}^{\mathrm{I}}}{G_{12}^{\mathrm{I}}}\right)^2 + \left(\frac{G_{23} - G_{23}^{\mathrm{I}}}{G_{23}^{\mathrm{I}}}\right)^2\\
&+ \left(\frac{\nu_{12} - \nu_{12}^{\mathrm{I}}}{\nu_{12}^{\mathrm{I}}}\right)^2 + \left(\frac{\nu_{23} - \nu_{23}^{\mathrm{I}}}{\nu_{23}^{\mathrm{I}}}\right)^2\Bigg].
\end{aligned} \tag{9}$$

In the previous equation, superscript "I" indicates the optimum value of the generic ply elastic property provided by the first-level inverse problem.

Also in this case, the second-level inverse problem can be formalised as a classical CNLPP:

Table 3
Second-level inverse problem: design variables lower and upper bounds.

Micro-scale elastic properties	Lower bound	Upper bound
E_1^f [MPa]	220800.0	331200.0
E_2^f [MPa]	13840.0	20760.0
ν_{12}^f	0.200	0.300
ν_{23}^f	0.343	0.514
G_{12}^f [MPa]	8992.0	13488.0
E_m [MPa]	3312.0	4968.0
ν_m^f	0.280	0.420

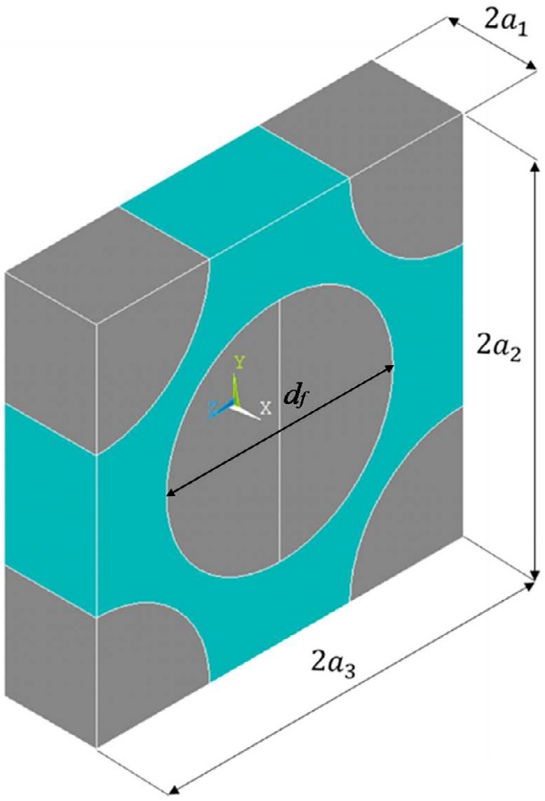

Fig. 6. The reference RVE.

$$\begin{aligned}
&\min_{\mathbf{x}^{II}} \Phi^{\mathrm{II}}(\mathbf{x}^{II}),\\
&\text{subject to:}\\
&g_j^{II}(\mathbf{x}^{II}) \leqslant 0, \quad j = 1, \ldots, 5.
\end{aligned} \tag{10}$$

4.2. The microscopic finite element model and the homogenisation strategy

The link between the microscopic and mesoscopic scales is represented by a homogenisation phase, performed on the RVE of Fig. 6. The lamina effective elastic properties are computed by means of the well-known strain energy homogenisation technique of periodic media described in [26]. This homogenisation scheme has proven to be an efficient numerical homogenisation procedure able to determine the equivalent material properties of different heterogeneous materials characterised by complex RVE topologies. The strain energy homogenisation technique of periodic media based on volume averaged stresses has already been used in other works, see [35,38–40].

The main hypothesis of this technique is that the repetitive unit of the periodic structure and the corresponding volume of the homogeneous solid undergo the same deformation having, hence, the same strain energy. At the mesoscopic scale (i.e. at the ply level), the heterogeneous medium is then replaced by an equivalent homogeneous anisotropic virtual material characterised by a set of elastic properties determined during the homogenisation phase. Of course, these properties depend upon the geometrical and material parameters of the RVE.

In this study, the real random micro-structure of the lamina (which is usually characterised by misalignments of the fibres, porosity, damaged zones, etc.) is not taken into account and the topology of the RVE is described by a perfect hexagonal array, as shown in Fig. 6.

The FE model of the RVE has been realised within the commercial FE code ANSYS®. A 20-nodes solid element (SOLID186) with three DOFs per node has been used. The model together with its structured

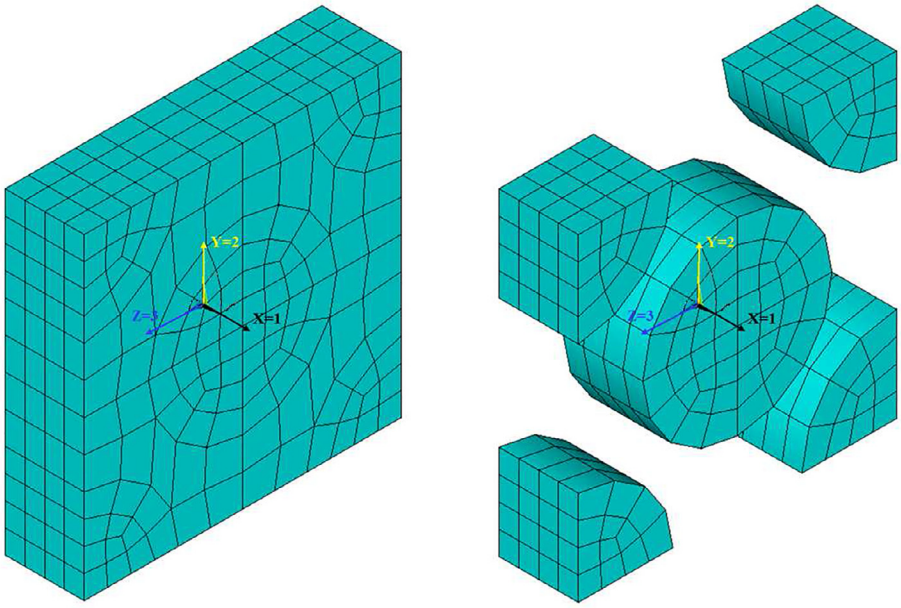

Fig. 7. FE model of the RVE, micro-scale.

mesh is illustrated in Fig. 7. Finally, a sensitivity study (not reported here for the sake of brevity) on the proposed FE model with respect to the mesh size has been conducted: it was observed that a mesh having 19551 DOFs is sufficient to properly evaluate the set of homogenised elastic properties at the mesoscopic scale.

In order to evaluate the components of the stiffness matrix [C] of the lamina, the RVE is submitted to an average strain field ε_{ij}^0 (tensor notation). The six components of the average strain are applied by considering the classical periodic boundary conditions (PBCs) on the RVE [26].

$$\begin{aligned} &u_i(a_1, x_2, x_3) - u_i(-a_1, x_2, x_3) = 2\cdot a_1\cdot\varepsilon_{i1}^0, \quad -a_2 \leqslant x_2 \leqslant a_2, -a_3 \leqslant x_3 \leqslant a_3,\\ &u_i(x_1, a_2, x_3) - u_i(x_1, -a_2, x_3) = 2\cdot a_2\cdot\varepsilon_{i2}^0, \quad -a_1 \leqslant x_1 \leqslant a_1, -a_3 \leqslant x_3 \leqslant a_3,\\ &u_i(x_1, x_2, a_3) - u_i(x_1, x_2, -a_3) = 2\cdot a_3\cdot\varepsilon_{i3}^0, \quad -a_1 \leqslant x_1 \leqslant a_1, -a_2 \leqslant x_2 \leqslant a_2,\\ &i = 1, 2, 3. \end{aligned} \tag{11}$$

The PBCs, shown in Eq. (11), result in a complex strain field inside the RVE. The applied average strains always meet the following condition (V denotes the RVE volume):

$$\bar{\varepsilon}_{ij} = \frac{1}{V}\cdot\int_V \varepsilon_{ij}\, dV = \varepsilon_{ij}^0. \tag{12}$$

For the homogeneous material at the upper scale, the relationship between average stress and strain (Voigt's notation) is:

$$\bar{\sigma}_\alpha = C_{\alpha\beta}\cdot\bar{\varepsilon}_\beta, \quad \alpha, \beta = 1, \ldots, 6. \tag{13}$$

In the previous equation the Einstein's summation convention on repeated indexes is tacitly assumed. The components of the stiffness matrix [C] are determined by solving six static analyses on the RVE and by imposing the previous PBCs, where only one component at time of the strain ε_β^0 is different from zero for each one of the six problems. For all the static analyses the volume-averaged value of the generic component of the stress field $\bar{\sigma}_\alpha$ can be easily computed and the stiffness matrix of the ply can be calculated one column at time:

$$\begin{aligned} C_{\alpha\beta} = \frac{\bar{\sigma}_\alpha}{\varepsilon_\beta^0} = \frac{1}{V\cdot\varepsilon_\beta^0}\cdot\int_V \sigma_\alpha(x_1, x_2, x_3)\, dV, \quad \alpha, \beta = 1, \ldots, 6;\ \varepsilon_\gamma^0 = 0, \quad \gamma \\ = 1, \cdots, 6, \quad \gamma \neq \beta. \end{aligned} \tag{14}$$

The engineering moduli of the constitutive lamina at the mesoscopic scale can be calculated starting from the components of the compliance matrix $[S] = [C]^{-1}$. For more details on the homogenisation procedure, the interested reader is addressed to [26].

4.3. The numerical strategy

Problem (10) is a non-convex CNLPP in terms of both constraint and objective functions, see Eqs. (8) and (9).

Concerning problem (10), the number of variables is equal to *seven*. The existence of the optimum solution may not be unique because the number of *observed states* is lower than that of design variables to be identified. Therefore, the transition from mesoscopic to microscopic scale is governed by non-bijective relationships which can give rise to a significant amount of equivalent optimum solutions for the problem at hand.

In order to find a solution for the second-level inverse problem, the two-step optimisation procedure is adapted to the transition from mesoscopic scale to microscopic one, as illustrated in Fig. 8.

For the resolution of the second-level inverse problem, the optimisation algorithm has been interfaced with the FE model of the RVE at micro-scale, to perform the numerical homogenisation. As stated above, the optimisation tool invokes the FE model of the material RVE on which six static analyses are performed: the PBCs allow determining the components of the ply stiffness tensor, for each individual at each generation.

Then, the optimisation tool elaborates the results provided by the FE analyses in order to execute the optimisation operations on the basis of the current values of both objective and constraint functions (both for the GA and the gradient algorithm). These operations are repeated until the user-defined convergence criterion is satisfied.

Concerning the GA, the genotype of the individual for problem (10) is characterised by only *one* chromosome composed of *seven* genes, each one coding a component of the vector of design variables of Eq. (7).

5. Numerical results

5.1. Determination of the harmonic response for the reference configuration

Before launching the optimisation process, the reference harmonic response must be determined. The geometry as well as the material properties of the reference configuration have been introduced in Section 2. The reference harmonic response is calculated by performing

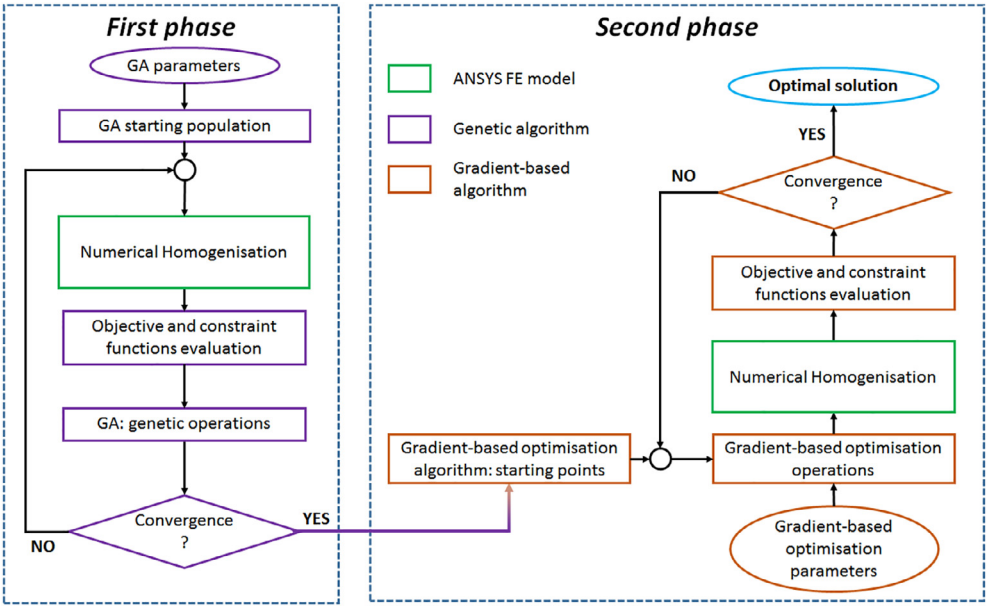

Fig. 8. Optimisation scheme for the second-level inverse problem.

Table 4
Reference values of the lamina material properties.

Ply properties						
E_1 [MPa]	E_2 [MPa]	ν_{12}	ν_{23}	G_{12} [MPa]	G_{23} [MPa]	ρ [kg/m^3]
s155028.4	8197.9	0.290	0.510	3837.1	3282.8	1770.0

two successive analyses (modal analysis followed by a linear harmonic one) on the macroscopic FE model of the multilayer plate discussed in Section 3. Of course, at the macroscopic scale both the reference FRF of the laminate and the set of reference natural frequencies have been calculated by using the geometrical properties of the reference structure and by considering the ply elastic properties listed in Table 4. These material parameters are obtained by means of a preliminary homogenisation analysis through the FE model of the RVE of the composite (see Section 4) in which the reference values of Table 1 for the elastic properties of both fibre and matrix are used.

The frequency samples used for the determination of the structure FRF vary between $f_{LB} = 500$ Hz and $f_{UB} = 6000$ Hz. $n_f = 8$ natural frequencies falls in this interval: they are extracted to evaluate the optimisation constraints of Eq. (4). Their reference values are listed in Table 5. The FRF of the multilayer plate is divided according to the sampling sequence summarised in Table 6. It must be noticed that the sampling intervals used for the definition of the FRF and, hence, of the objective function of the first-level inverse problem of Eq. (3), have been properly parametrized in terms of the current value of the

Table 5
Reference natural frequencies.

Nat. freq.	Value [Hz]
f_{1n}^{ref}	760.98
f_{2n}^{ref}	1847.19
f_{3n}^{ref}	1997.35
f_{4n}^{ref}	2966.36
f_{5n}^{ref}	3770.59
f_{6n}^{ref}	3856.76
f_{7n}^{ref}	4605.93
f_{8n}^{ref}	5061.77

Table 6
Sampling sequence for FRF calculation ($\delta = 1$ Hz).

Frequency intervals [Hz]	N. of sampled spectrum points
$\left[1-\frac{f_{1n}^{\text{ref}}-f_{LB}}{f_{1n}^{\text{ref}}}\right]f_{1n} < f < f_{1n}-\delta$	6
$f_{1n}+\delta < f < f_{2n}-\delta$	10
$f_{2n}+\delta < f < f_{3n}-\delta$	10
$f_{3n}+\delta < f < f_{4n}-\delta$	10
$f_{4n}+\delta < f < f_{5n}-\delta$	10
$f_{5n}+\delta < f < f_{6n}-\delta$	10
$f_{6n}+\delta < f < f_{7n}-\delta$	10
$f_{7n}+\delta < f < f_{8n}-\delta$	10
$f_{8n}+\delta < f < \left[1-\frac{f_{UB}-f_{8n}^{\text{ref}}}{f_{8n}^{\text{ref}}}\right]f_{8n}$	6

structure natural frequencies f_{jn}, $(j = 1, \ldots, n_f)$. Moreover, since damping is neglected, a small range of frequencies in the neighbourhood of each natural frequency f_{jn} (by considering a "small" interval of length $\delta = 1$ Hz centred at each natural frequency) has been excluded from the sampling sequence. The exciting nodal force has a value $F_z = 1\ N$.

Finally, as discussed in Section 3, the FRF is calculated at each one of the 62 reference points defined over the laminate, as illustrated in Fig. 4.

5.2. Results of the first-level inverse problem (meso-scale)

In this section, the results of the first-level inverse problem are shown and discussed. After carrying out a statistic analysis in order to evaluate the effect of the optimisation parameters on the optimum solutions, according to [38], the main parameters tuning the behaviour of both the GA and the active-set algorithm (used to carry out global and local optimisation, respectively) are set as listed in Tables 7 and 8.

For this first case, the GA makes use of two populations with 60 individuals evolving along 130 generations. The exchange of information among populations is performed through a ring-type operator every 10 generations, with a probability which is automatically evaluated by the GA itself. Moreover, concerning the constraint-handling technique for the first-level inverse problem, the Automatic Dynamic Penalisation (ADP) method has been considered, see [41].

Table 7
Genetic algorithm parameters (for both first-level and second-level inverse problems).

Parameters	First-level	Second-level
N. of individuals	120	140
N. of populations	2	2
N. of iterations	130	130
Crossover probability.	0.85	0.85
Mutation probability.	0.06	0.07
Isolation time	10	10

Table 8
Gradient-based algorithm parameters (for both first-level and second-level inverse problems).

Parameters	Value
Solver algorithm	Active-set
Max function evaluation	10000
Tolerance on the objective function	10^{-15}
Tolerance on the gradient norm	10^{-15}

The choice of using multiple populations of small size, i.e. with a small number of individuals, is motivated by the fact that here the goal is to find the global minimum (for the objective function of the problem at hand) without increasing too much the computational effort. Indeed, the exchange of information between best individuals belonging to different populations (through the use of the ring-type operator), and hence the possibility of crossing them, allows the GA for exploring the feasible design domain and for handling the genetic information in the best way. More details about the use of multiple populations can be found in [25]. For the first-level inverse problem, the single numerical harmonic analysis (which must be performed for each individual at each iteration) needs about 30 s to be executed (on an Intel® Xeon® 2.70 GHz CPU with two processors and with a RAM of 128 GB), which implies an overall time of about 8.3 days to get an optimum solution.

The optimum solutions found at the end of both the genetic calculation and the local gradient-based optimisation are summarised in Table 9, whilst the values of the eigenfrequencies for the optimum solution are given in Table 10.

The FRF of the optimum solution evaluated in four different nodes (nodes 40, 447, 501 and 660 according to Fig. 4) are illustrated in Fig. 9.

As it can be easily inferred from the analysis of these results, the ply elastic properties of the optimum solution are in good agreement with the reference data: the absolute percentage difference ranges from 0% for G_{12} to 5.78% for ν_{23}. This is a quite expected result because, due to the kinematic model at the basis of ANSYS shell elements (first-order shear deformation theory), the effect of ν_{23} on both the displacement field and the natural frequencies is negligible. The plate is not thick enough to observe a significant influence of ν_{23} on its dynamic response.

Table 9
Optimum solution of the first-level inverse problem provided by the GA and the gradient-based algorithm; the percentage difference between the solution and the ply reference data are given in parentheses.

Meso-scale elastic properties	Reference data	GA results	Gradient-based results
E_1 [MPa]	155028.4	153846.0 (−0.762)	155027.5 (-6.45×10^{-04})
E_2 [MPa]	8197.9	8103.3 (−1.15)	8197.7(-1.95×10^{-03})
ν_{12}	0.290	0.284 (−1.94)	0.290 (3.45×10^{-03})
ν_{23}	0.510	0.480 (−5.76)	0.480 (−5.78)
G_{12} [MPa]	3837.1	3906.9 (1.82)	3837.1 (0)
G_{23} [MPa]	3282.8	3291.1 (0.254)	3282.5 (-7.62×10^{-03})

Table 10
First eight natural frequencies for the optimum solution of the first-level inverse problem; for each value, the percentage difference with respect to the reference counterpart is indicated in parentheses.

Nat. freq.	f_{in}^{ref} [Hz]	f_{in} [Hz]
f_{1n}	760.98	760.97 (3.51×10^{-04})
f_{2n}	1847.19	1847.18 (3.82×10^{-04})
f_{3n}	1997.35	1997.34 (3.83×10^{-04})
f_{4n}	2966.36	2966.34 (3.99×10^{-04})
f_{5n}	3770.59	3770.57 (4.20×10^{-04})
f_{6n}	3856.76	3856.74 (4.23×10^{-04})
f_{7n}	4605.93	4605.91 (4.27×10^{-04})
f_{8n}	5061.77	5061.74 (4.58×10^{-04})

Nevertheless, both the eigenfrequencies and the FRF, in all sample points, are very well estimated. The numerical results found at the end of the optimisation perfectly match the reference data with an absolute percentage difference ranging from 3.51×10^{-4}% (for the 1-*th* mode) to 4.58×10^{-4}% (for the 8-*th* mode).

Finally, the utilisation of the active-set method really improves the quality of the pseudo-optimal solution provided by the GA: the value of the objective function decreases from 4.29×10^{-4}, at the end of the genetic calculation to 6.00×10^{-7}, at the end of the local optimisation.

5.3. Results of the second-level inverse problem (micro-scale)

The second-level inverse problem is solved by considering a fibre volume fraction $V_F = 0.555$ [27] and a fibre diameter equal to $d_f = 6.8\ \mu\text{m}$ [42].

The RVE dimensions are obtained as follows:

$$a_3 = \frac{d_f}{4}\sqrt{\frac{2\pi}{V_f}}, \quad a_2 = a_3, \quad a_1 = a_2/4. \tag{15}$$

The parameters tuning the behaviour of both the GA and the active-set algorithm for the second-level inverse problem are listed in Tables 7 and 8. As in the case of the first-level inverse problem, the Automatic Dynamic Penalisation (ADP) method has been considered for handling constraints [41]. As far as the second-level inverse problem is concerned, the optimisation process is faster: about 2.3 days are required to find a solution because the set of 6 static analyses to be conducted on the composite RVE needs only 6 s (and they must be performed for each point in the design space).

The optimum solutions of the second-level problem found at the end of both the genetic calculation and the local gradient-based optimisation are summarised in Tables 11 and 12.

As it can be easily inferred from the analysis of these results, the elastic properties of the constitutive phases for the optimum solution are in agreement with the reference data. In particular, Young's and shear moduli for both fibre and matrix are estimated with a very good accuracy: the absolute percentage difference ranges from 0.254% for E_1^f to 5.56% for E_2^f.

Conversely, the estimation of the Poisson's ratio (for both phases) is characterised by a higher discrepancy: the maximum absolute percentage difference is 13.4% on ν_{23}^f. However, this is a quite expected result because, as stated above, the Poisson's ratio ν_{23} of the lamina has a negligible influence on the laminate dynamic response. Indeed, the related sensitivity of both objective and constraint functions of the first-level problem to the variable ν_{23} is not significant at all. Therefore, the relatively small absolute percentage error on ν_{23} at the end of the first-level inverse problem (5.78%) is amplified when looking for the optimum solution of the second-level inverse problem in terms of Poisson's ratios of both fibre and matrix (the associated optimisation problem is non-linear).

Finally, the quality of the optimum solution of the second-level

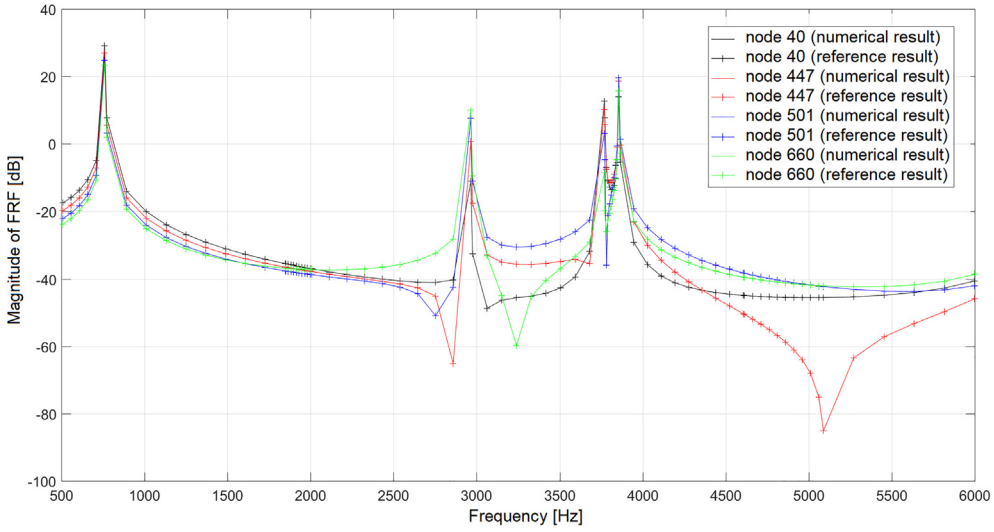

Fig. 9. Example of FRF for both optimum and reference solutions evaluated at nodes 40, 447, 501 and 660.

Table 11
Optimum solution of the second-level inverse problem provided by both the GA and the active-set algorithm; the percentage difference between the solution and the reference material properties are given in parentheses.

Micro-scale elastic properties	Reference data	GA results	Gradient-based results
E_1^f [MPa]	276000.0	276701.0 (0.254)	276701.0 (0.254)
E_2^f [MPa]	17300.0	18277.5 (5.65)	18262.1 (5.56)
ν_{12}^f	0.250	0.274 (9.76)	0.275 (9.83)
ν_{23}^f	0.428	0.487 (13.6)	0.486 (13.4)
G_{12}^f [MPa]	11240.0	10807.1 (−3.85)	10780.7 (−4.09)
E_m [MPa]	4140.0	4108.4 (−0.763)	4108.4 (−0.763)
ν_m	0.350	0.315 (−9.99)	0.315 (−9.99)

Table 12
Ply material properties at the end of the first-level inverse problem (used as target values) and those related to the optimum solution resulting from the second-level inverse problem; the percentage differences are indicated in parentheses.

Ply elastic properties	First-level problem results	Optimum results
E_1 [MPa]	155027.5	155392.0 (0.235)
E_2 [MPa]	8197.7	8170.8 (−0.328)
ν_{12}	0.290	0.290 (0.0)
ν_{23}	0.480	0.480 (0.0)
G_{12} [MPa]	3837.1	3837.2 (2.87×10^{-3})
G_{23} [MPa]	3282.5	3289.0 (0.196)

inverse problem is very good: the objective function value is 2.0519×10^{-5} at the end of the local gradient-based optimisation.

6. Conclusions and perspectives

In this work a multi-scale identification strategy (MSIS) able to characterise the elastic properties of composite materials, at each characteristic scale, is presented. The MSIS is characterised by several original features that make it a very general methodology for characterising the elastic properties of anisotropic media.

In the context of the MSIS, the problem of characterising the elastic properties of the composite at different scales is split into two distinct (but related) *inverse problems*. The first-level inverse problem involves the transition from macroscopic scale (laminate-level) to mesoscopic one (ply-level): the goal is to characterise the ply elastic properties minimising the distance between the numerical harmonic response of the multilayer plate and the reference one. Conversely, the second-level inverse problem focuses on the transition from mesoscopic scale to microscopic one (that of the constitutive phases): the goal is to find the optimum value of elastic properties of both fibre and matrix matching the set of the lamina elastic properties provided by the first-level problem.

The overall identification process relies on a single non-destructive harmonic test performed at the macroscopic scale. The MSIS makes use of the strain energy homogenisation technique of periodic media to carry out the scale transition (from microscopic to mesosocopic one) as well as of a hybrid optimisation tool to perform the solution search for both first-level and second-level inverse problems.

The effectiveness of the MSIS is evaluated through a numerical benchmark: a multilayer plate made of unidirectional carbon/epoxy pre-preg plies $T650/F584$, whose elastic properties are taken from literature, is considered as a reference structure and its harmonic response has been taken as a reference one.

At the mesoscopic scale (ply-level) the results of the identification process are very good: the maximum absolute percentage error is observed on the ply transverse Poisson's ratio ν_{23} and is about 5.78%. At the microscopic scale (constitutive phases-level) all elastic properties are identified with a good level of accuracy, except the fibre and matrix Poisson's ratios: those of the fibre, i.e. $\nu_{12}^f$and ν_{23}^f, are affected by a absolute percentage error of about 10% and 14%, respectively, whilst that of the matrix, ν^m, is characterised by a percentage error of about 10%.

On the one hand, the relatively small error on the transverse Poisson's ratio of the lamina is due to the very low sensitivity of the objective function to this material property (the laminate is not thick enough). On the other hand, this error propagates at the lower scale and affect the Poisson's ratios of both fibre and matrix for which the percentage error is amplified (the problem is non-linear).

Nevertheless, thanks to the proposed multi-scale identification approach, it is possible to retrieve both longitudinal and transversal effective properties of the constitutive phases of the RVE and this task cannot be easily performed by means of standard ASTM tests. Moreover, such a result has been obtained by using a unique macroscopic non-destructive harmonic test.

The proposed strategy constitutes just a "first attempt": the methodology must be generalised and improved in order to catch the true behaviour of the material of the constitutive phases at the microscopic scale. To this purpose, research is ongoing in order to include into the MSIS the following aspects: on the one hand, the viscoelastic behaviour

of both fibre and matrix in order to validate the effectiveness of the approach by means of a comparison with experimental harmonic tests; on the other hand, the variability effects induced by the manufacturing process, e.g. local variation of the fibre volume fraction, misalignments of fibres, variation of the plies orientation angles, etc.

Of course, the integration of the viscoelastic behaviour of the matrix at the microscopic scale has three main consequences:

- the equivalent elastic properties of the constitutive lamina at the mesoscopic scale will depend upon the frequency;
- since the ply elastic properties depends upon the frequency, the problem of determining the structure natural frequencies becomes a non-linear eigenvalue problem, thus a suitable iterative method must be foreseen to perform the related modal analysis;
- the harmonic response of the laminate, at the macroscopic scale, will be strongly affected by the matrix viscoelastic behaviour; in particular, the eigenfrequencies values reduce (when compared to the undamped modal analysis) and the amplitude of the FRF take a finite value (instead of an infinite one) when the frequency of the applied load/displacement is equal to the generic damped natural frequency.

In this context, the MSIS presented in this work can be used, on the one hand, to characterise the parameters of the law tuning the matrix viscoelastic behaviour and, on the other hand, to select the mathematical model which fits best the true viscoelastic behaviour, for a given frequency range

Finally, thanks to the versatility of the proposed MSIS, it is possible to characterise the geometrical features of the RVE of the composite material: the parameters defining the shape of the inclusion or its volume fraction can be easily integrated among the optimisation variables, without altering the overall architecture of the identification methodology. On the other hand, also geometric parameters of the laminate (mesoscopic scale) can be included among the unknowns to be identified, e.g. the orientation angles and the thickness of each lamina. Research is ongoing on these aspects as well.

Acknowledgements

This research work has been carried out within the project FULLCOMP (FULLy analysis, design, manufacturing, and health monitoring of COMPosite structures), funded by the European Union Horizon 2020 Research and Innovation program under the Marie Skodowska-Curie grant agreement No. 6421211.

Appendix A. Supplementary data

Supplementary data associated with this article can be found, in the online version, athttps://doi.org/10.1016/j.compstruct.2018.08.007.

References

[1] Adams FD, Carlsson AL, pipes RB. Experimental characterization of advanced composite materials. 3rd ed. CRC Press LLC; 2003.
[2] Maurin R, Davies P, Baral N, Baley C. Transverse properties of carbon fibres by nano-indentation and micro-mechanics. Appl Compos Mater 2018;15:61–73.
[3] ASTM International, West Conshohocken, PA, ASTM D3039/D3039M-17. Standard Test Method for Tensile Properties of Polymer Matrix Composite Materials; 2017.
[4] ASTM International, West Conshohocken, PA, ASTM D790-17. Standard test methods for flexural properties of unreinforced and reinforced plastics and electrical insulating materials; 2017.
[5] ASTM International, West Conshohocken, PA, ASTM D3410/D3410M-16. Standard test method for compressive properties of polymer matrix composite materials with unsupported gage section by shear loading; 2016.
[6] ASTM International, West Conshohocken, PA, ASTM D695-15. Standard test method for compressive properties of rigid plastics; 2015.
[7] ASTM International, West Conshohocken, PA, ASTM D6641/D6641M-16e1. Standard test method for compressive properties of polymer matrix composite materials using a combined loading compression (CLC) test fixture; 2016.
[8] ASTM International, West Conshohocken, PA, ASTM D5379/D5379M-12. Standard test method for shear properties of composite materials by the V-notched beam method; 2012.
[9] ASTM International, West Conshohocken, PA, ASTM D7078/D7078M-12. Standard test method for shear properties of composite materials by V-notched rail shear method; 2012.
[10] ASTM International, West Conshohocken, PA, ASTM D3518/D3518M-13. Standard test method for in-plane shear response of polymer matrix composite materials by tensile test of a laminate; 2013.
[11] ASTM International, West Conshohocken, PA, ASTM D2344/D2344M-16. Standard test method for short-beam strength of polymer matrix composite materials and their laminates; 2016.
[12] ASTM International, West Conshohocken, PA, ASTM D3379-75(1989) e1. Standard test method for tensile strength and young's modulus for high-modulus single-filament materials (Withdrawn 1998); 1975.
[13] ASTM International, West Conshohocken, PA, ASTM D638-14. Standard test method for tensile properties of plastics; 2014.
[14] Nairn JA. Analytical fracture mechanics analysis of the pull-out test including the effects of friction and thermal stresses. Adv Compos Lett 2000;9(6):373–83.
[15] Feih S, Wonsyld K, Minzari D, Westermann P, Lilholt H. Testing procedure for the single fiber fragmentation test, Vol. No. 1483(EN), Denmark. Risoe-R: Forskningscenter Risoe; 2004.
[16] Young TJ. Characterisation of interfaces in micro- and nano-composites. University of Surrey; 2012. [Ph.D. thesis].
[17] Lee C, Kam T. Identification of mechanical properties of elastically restrained laminated composite plates using vibration data. J Sound Vib 2006;295:999–1016.
[18] Xing L, Zhidong G, Zengshan L, Lu L. A new stress-based multi-scale failure criterion of composites and its validation in open hole tension tests. Chin J Aeronaut 2014;27(6):1430–41.
[19] Andy V, Brian CN, Stepan L, Dirk V. Multi-scale modelling strategy for textile composites based on stochastic reinforcement geometry. Comput Methods Appl Mech Eng 2016;310:906–34.
[20] Furtado S, Araujo A, Silva A. Inverse characterization of vegetable fibre-reinforced composites exposed to environmental degradation. Compos Struct 2018;189:529–44.
[21] Zhou X-Y, Gosling PD, Ullah Z, Kaczmarczyk L, Pearce C. Exploiting the benefits of multi-scale analysis in reliability analysis for composite structures. Compos Struct 2016;155:197–212.
[22] Pedersen P. Identification techniques in composite laminates. NATO ASI Ser E Appl Sci 1999;361:443–52.
[23] Pedersen P, Frederiksen PS. Identification of orthotropic material modul by a combined experimental/numerical method. Measurement 1992;10(3):113–8.
[24] Mota Soares CM, Moreira de Freitas M, Aro AL, Pedersen P. Identification of material properties of composite plate specimens. Compos Struct 1993;25:277–85.
[25] Montemurro M. Optimal design of advanced engineering modular systems through a new genetic approach. Paris VI, France: UPMC; 2012. [Ph.D. thesis],http://tel.archives-ouvertes.fr/tel-00955533.
[26] Barbero E. Finite element analysis of composite materials. CRC Press, Taylor and Francis Group; 2007.
[27] Soutis C, Beaumont PWR, editors. Multi-scale modelling of composite material systems. The art of predictive damage modelling, Woodhead Publishing Series in Composites Science and Engineering New York: Elsevier; 2005.
[28] Corporation Hexcell. Hexply 2016;F584.
[29] Ansys. ANSYS Mechanical APDL Basic Analysis Guide. Release 15.0, ANSYS Inc, Southpointe, 275 Technology Drive, Canonsburg, PA 15317; 2013.
[30] Jones RM. Mechanics of composite materials. McGraw-Hill; 1975.
[31] Sun N-Z. Inverse problems in groundwater modelling. Boston 6 of Theory and Applications of Transport in Porous Media; Kluwer Academic Publishers.
[32] Tarantola A. Inverse problem theory: methods for data fitting and model parameter estimation. New York: Elsevier; 1988.
[33] Costa G, Montemurro M, Pailhs J. A general hybrid optimization strategy for curve fitting in the non-uniform rational basis spline framework. J Optim Theory Appl 2018;176(1):225–51.
[34] The MathWorks Inc. 3 Apple Ill Drive, Natick, MA 01760-2098, Optimization Toolbox User's Guide; 2017.
[35] Montemurro M, Catapano A, Doroszewski D. A multi-scale approach for the simultaneous shape and material optimisation of sandwich panels with cellular core. Compos Part B: Eng 2016;91:458–72.
[36] Montemurro M, Catapano A. Variational analysis and aerospace engineering: mathematical challenges for the aerospace of the future. In: Springer Optimization and Its Applications, Springer International Publishing, 2016, Ch. A new paradigm for the optimum design of variable angle tow laminates, 1st ed., vol. 116, pp. 375–400.https://doi.org/10.1007/978-3-319-45680-5.
[37] Montemurro M, Catapano A. On the effective integration of manufacturability constraints within the multi-scale methodology for designing variable angle-tow laminates. Compos Struct 2017;161:145–59.
[38] Montemurro M, Nasser H, Koutsawa Y, Belouettar S, Vincenti A, Vannucci P. Identification of electromechanical properties of piezoelectric structures through evolutionary optimisation techniques. Int J Solids Struct 2012;49(13):1884–92.
[39] Catapano A, Montemurro M. A multi-scale approach for the optimum design of sandwich plates with honeycomb core, Part I: homogenisation of core properties. Compos Struct 2014;118:664–76.
[40] Catapano A, Montemurro M. A multi-scale approach for the optimum design of sandwich plates with honeycomb core, Part II: the optimisation strategy. Compos Struct 2014;118:677–90.
[41] Montemurro M, Vincenti A, Vannucci P. The automatic dynamic penalisation method (ADP) for handling constraints with genetic algorithms. Comput Methods Appl Mech Eng 2013;256:70–87.
[42] Cytec Industries Inc. THORNEL T-650/35 Pan-based fiber; 2012.